In Vivo Imaging of Amyloid Deposition in Alzheimer Disease Using the Radioligand ^{18}F-AV-45 (Flobetapir F 18)

Dean F. Wong[1–4], Paul B. Rosenberg[2,5], Yun Zhou[1], Anil Kumar[1], Vanessa Raymont[1], Hayden T. Ravert[1], Robert F. Dannals[1], Ayon Nandi[1], James R. Brašić[1], Weiguo Ye[1], John Hilton[1], Constantine Lyketsos[2,5,6], Hank F. Kung[7], Abhinay D. Joshi[8], Daniel M. Skovronsky[7,8], and Michael J. Pontecorvo[8]

[1]Section of High Resolution Brain PET Imaging, Division of Nuclear Medicine, Russell H. Morgan Department of Radiology and Radiological Science, Johns Hopkins Medical Institutions, Baltimore, Maryland; [2]Department of Psychiatry and Behavioral Sciences, Johns Hopkins Medical Institutions, Baltimore, Maryland; [3]Solomon H. Snyder Department of Neuroscience, Johns Hopkins University School of Medicine, Johns Hopkins Medical Institutions, Baltimore, Maryland; [4]Department of Environmental Health Sciences, Johns Hopkins University Bloomberg School of Public Health, Johns Hopkins Medical Institutions, Baltimore, Maryland; [5]Memory and Alzheimer's Treatment Center, Johns Hopkins Medical Institutions, Baltimore, Maryland; [6]Department of Mental Health, Johns Hopkins University Bloomberg School of Public Health, Baltimore, Maryland; [7]Department of Radiology, University of Pennsylvania, Philadelphia, Pennsylvania; and [8]Avid Radiopharmaceuticals, Inc., Philadelphia, Pennsylvania

An ^{18}F-labeled PET amyloid-β (Aβ) imaging agent could facilitate the clinical evaluation of late-life cognitive impairment by providing an objective measure for Alzheimer disease (AD) pathology. Here we present the results of a clinical trial with (E)-4-(2-(6-(2-(2-(2-^{18}F-fluoroethoxy)ethoxy)ethoxy)pyridin-3-yl)vinyl)-N-methyl benzenamine (^{18}F-AV-45 or flobetapir F 18). **Methods:** An open-label, multicenter brain imaging, metabolism, and safety study of ^{18}F-AV-45 was performed on 16 patients with AD (Mini-Mental State Examination score, 19.3 ± 3.1; mean age ± SD, 75.8 ± 9.2 y) and 16 cognitively healthy controls (HCs) (Mini-Mental State Examination score, 29.8 ± 0.45; mean age ± SD, 72.5 ± 11.6 y). Dynamic PET was performed over a period of approximately 90 min after injection of the tracer (370 MBq [10 mCi]). Standardized uptake values and cortical-to-cerebellum standardized uptake value ratios (SUVRs) were calculated. A simplified reference tissue method was used to generate distribution volume ratio (DVR) parametric maps for a subset of subjects. **Results:** Valid PET data were available for 11 AD patients and 15 HCs. ^{18}F-AV-45 accumulated in cortical regions expected to be high in Aβ deposition (e.g., precuneus and frontal and temporal cortices) in AD patients; minimal accumulation of the tracer was seen in cortical regions of HCs. The cortical-to-cerebellar SUVRs in AD patients showed continual substantial increases through 30 min after administration, reaching a plateau within 50 min. The 10-min period from 50 to 60 min after administration was taken as a representative sample for further analysis. The cortical average SUVR for this period was 1.67 ± 0.175 for patients with AD versus 1.25 ± 0.177 for HCs. Spatially normalized DVRs generated from PET dynamic scans were highly correlated with SUVR (r = 0.58–0.88, P < 0.005) and were significantly greater for AD patients than for HCs in cortical regions but not in subcortical white matter or cerebellar regions. No clinically significant changes in vital signs, electrocardiogram, or laboratory values were observed. **Conclusion:** ^{18}F-AV-45 was well tolerated, and PET showed significant discrimination between AD patients and HCs, using either a parametric reference region method (DVR) or a simplified SUVR calculated from 10 min of scanning 50–60 min after ^{18}F-AV-45 administration.

Key Words: Aβ; PET; Alzheimer disease; dementia; biomarkers; aging; [18]F

Although the etiology of Alzheimer disease (AD) has not been established, converging evidence suggests that the amyloid-β (Aβ) peptide plays an important role in AD pathogenesis (1). Plaques containing Aβ fibrils are found in the AD brain and are a key component of the neuropathologic criteria for autopsy-based confirmation of diagnosis (2,3). Immunologic therapies that decrease Aβ deposition have been shown to stabilize or reverse cognitive deficits in transgenic mouse models of AD (4). Additionally, Aβ deposition is thought to precede cognitive symptoms in AD and is a potential preclinical marker of disease (5). Thus, Aβ deposition is a major target for novel AD treatments currently in human trials.

However, these efforts have been hampered by the absence of reliable, noninvasive markers for brain Aβ load. A reliable biomarker could aid diagnosis by documenting the presence of disease-specific pathology and could be useful for the prediction of postdisease progression, evaluation of effects of therapy on disease progression, and presymptomatic identification of subjects at risk for developing

AD. Although cerebrospinal fluid Aβ levels are reliably decreased in AD (6), cerebrospinal fluid studies are inevitably indirect markers. Imaging techniques using radiolabeled PET tracers that bind to the aggregated Aβ peptides in Aβ plaques have the potential to directly assess relative brain Aβ plaque pathology. To date, the most widely researched imaging approach has used the ^{11}C-labeled PET tracer [N-methyl-]2-(4′-methylaminophenyl)-6-hydroxybenzothiazole (6-OH-BTA), also known as Pittsburgh compound B or PIB (7). Despite these encouraging results, the short half-life (20 min) of the ^{11}C isotope may limit the utility of ^{11}C-PIB as a tool for aiding in community-based diagnosis and therapeutic evaluation.

Because ^{18}F has a radioactive half-life of 110 min, regional preparation and shipping of doses is possible, thereby reducing the cost and greatly increasing the number of potential imaging center users. Several ^{18}F-labeled Aβ tracers have been successfully tested in clinical trials (Supplemental Fig. 1; supplemental materials are available online only at http://jnm.snmjournals.org) (8–10). However, a ligand with faster kinetics was desired to enable shorter imaging procedures of AD patients. (E)-4-(2-(6-(2-(2-(2-^{18}F-fluoroethoxy)ethoxy)ethoxy)pyridin-3-yl)vinyl)-N-methyl benzenamine (^{18}F-AV-45 or flobetapir F 18) was selected from a series of agents as the tracer with the optimum kinetics and selectivity for Aβ plaques (11). The present study was designed as a preliminary exploration of the brain-imaging properties, pharmacokinetics, and tolerability of ^{18}F-AV-45 (flobetapir F 18) in elderly cognitively healthy controls (HCs) and in patients with AD.

MATERIALS AND METHODS

^{18}F-AV-45 (flobetapir F 18) was studied at 3 sites—Johns Hopkins Hospital/Johns Hopkins University (JHU), Memory Enhancement Center of America, Long Branch, NJ, and Community Health Research, North East, MD—in elderly subjects who were cognitively healthy and patients with AD.

Eligibility and Overall Study Design

^{18}F-AV-45 was studied in a total of 16 HC volunteers and 16 AD patients. Patients with AD had to be older than 50 y and have a probable diagnosis of AD according to the National Institute of Neurological and Communicative Disorders and Stroke and the Alzheimer's Disease and Related Disorders Association, with a Mini-Mental State Examination (MMSE) score of between 10 and 24, inclusively (12,13). HCs had to be older than 50 y, with no evidence of cognitive impairment by history and psychometric testing, and had to have an MMSE score of at least 29. Subjects who showed evidence of any other significant neurodegenerative or psychiatric disease on clinical examination or MRI or clinically significant medical comorbidities that might pose a safety risk to the subject or interfere with interpretation of the scan were excluded from the study. Patients with AD could be on a stable dose (by investigator judgment: not in titration period, no change in medication being considered) of an acetylcholinesterase inhibitor, memantine, or vitamin E. Patients who had participated in an experimental study with a treatment that targeted Aβ (e.g., immunotherapy, secretase inhibitor, selective Aβ-lowering agents)

were excluded. All procedures were approved by the appropriate Institutional Review Board, and all participants or an appropriate representative signed informed consent forms, consistent with established criteria (12).

Similar acquisition protocols were used at the 3 centers. All subjects received a single intravenous bolus of approximately 370 MBq (10 mCi) of ^{18}F-AV-45, and PET began. Dynamic brain PET images were collected for approximately 90 min. The PET scanners used were the Advance (GE Healthcare) (PET only, at JHU), Discovery LS (GE Healthcare) (PET/CT, at Community Health Center and The Memory Enhancement Center), and Discovery ST (GE Healthcare) (PET/CT, at The Memory Enhancement Center). In addition, plasma metabolites were analyzed using the method of Hilton et al. (14). The supplemental information provides detailed PET, metabolite analysis, and image-acquisition procedures.

Radiosynthesis of ^{18}F-AV-45

The doses of ^{18}F-AV-45 were prepared individually on the day of administration at either the JHU cyclotron or radiochemistry laboratory or at the Avid Radiopharmaceuticals radiochemistry laboratory in accordance with the Avid Radiopharmaceuticals Investigational New Drug master batch record and quality control release criteria. Mean specific activity at the time of injection was 74,777 ± 72,409 GBq/mmol (2,021 ± 1,957 Ci/mmol).

Image Analysis

Computation of Standardized Uptake Values (SUVs) and SUV Ratios (SUVRs)—All Subjects. PET images for each subject were resliced (realigned) to create a mean image across all frames (individual acquisition time blocks). This image was normalized to Talairach space by SPM (version 2; Wellcome Trust Centre for Neuroimaging). Each individual frame was then fitted to this normalized mean image. No partial-volume correction was performed. To identify volumes of interest (VOIs) for analysis, images of 10 subjects were segmented to identify gray and white matter, cerebrospinal fluid, and skull. Images from the first 10 min after administration in the first 15 subjects were then analyzed, and high-flow areas were determined and compared with the previously segmented gray matter dataset. VOIs were created in the high-flow regions of the frontal, temporal, parietal, occipital, anterior cingulate, posterior cingulate, and precuneus cortical gray matter, and counts were extracted. SUVs were then generated from the VOI for each time frame. SUVRs were calculated using cerebellar gray matter as the primary reference region and centrum semiovale white matter as an alternative reference region.

Mathematic Kinetic Modeling (for Distribution Volume Ratio [DVR] Measures)

In a subset of subjects (9 AD patients and 8 HCs) for whom adequate MRI scans were available, time–activity curves were presented as percentage injected dose and kBq/cm^3 for kinetic analyses. A parametric mapping approach with the cerebellum as a reference region (15) was used to calculate DVRs (16).

Whole-Body Imaging and Dosimetry Estimation

Because this was an exploratory, first-in-humans study, brain imaging in 4 healthy subjects was interrupted, and whole-body scans were obtained for preliminary dosimetry estimation from approximately 20 to 45 min after administration of the dose and again from approximately 160 to 185 min after administration of the dose. One subject's data were not available because of

technical problems with image retrieval. Data were fit using the SAAM II software (*17*). Time integrals of activity (*18*) were entered into the OLINDA/EXM software (*19*) using the adult male model. Urinary and intestinal tract excretion data were treated with the OLINDA/EXM urinary bladder and International Commission on Radiological Protection gastrointestinal tract model (*20*).

RESULTS

Subjects

Thirty-two subjects were injected with the imaging agent (16 elderly HCs and 16 AD patients). Baseline characteristics are summarized in Table 1. The first human study worldwide was performed at Johns Hopkins University on June 8, 2007.

The mean radioactivity injected was 381.1 ± 41.07 MBq (10.3 ± 1.11 mCi) in the AD patients and 358.9 ± 40.7 MBq (9.7 ± 1.1 mCi) in HCs. As would be expected, the baseline average MMSE was lower in the AD patients than in the HCs (19.1 ± 3.1 vs. 29.8 ± 0.45). The AD and HC groups were similar in age, weight, and education. A slightly higher proportion of men composed the HC than in the AD group (10/16 vs. 8/16, respectively). Despite the mass dose range (0.56–9.1 μg), no correlation with SUVR for AD, HC, or the combination of the two was observed.

All elderly HCs and 15 of 16 (94%) AD patients completed the study. One AD patient (6.3%) withdrew consent after 5 min in the scanner. All subjects who received ^{18}F-AV-45 for injection were included in the safety analysis. Efficacy was analyzed for subjects who underwent PET for at least 10 min and had no significant technical failures in the imaging session. Technical failures occurred in 5 subjects. Four of the 5 technical failures occurred in AD patients who exhibited poor placement or excessive movement while in the scanner, which limited proper attenuation correction and quantification of the results. For the fifth subject, operational difficulties with the scanner precluded reconstruction of the data, and no usable images were obtained from the scanner. Thus, valid data for the evaluable population were available for 15 HCs and 11 AD patients.

TABLE 1. Demographics: All Subjects, All 3 Centers

Demographic	AD patients	HCs
n	16	16
Age (y)	75.8 ± 9.2	72.5 ± 11.6
MMSE*	19.3 ± 3.1	29.8 ± 0.5
Weight (kg)	75.4 ± 20	82.0 ± 15
Sex (M/F)	8/8	10/6
College education	12/16 (75%)	12/16 (75%)
Duration symptoms (mo)	70.6 ± 35	0

*MMSE scores for AD patients vs. HCs were significantly different by simple 2-tailed *t* test, $P < 0.001$.

Data are mean ± SD or numbers of patients.

Imaging Results

Figure 1 shows a typical image from an AD patient and HC subject. These count ratio (SUVR) images were averaged across two 5-min frames, beginning 50 min after the intravenous administration of ^{18}F-AV-45. Each voxel was divided by the average number of counts per voxel in the cerebellar gray matter.

In the AD patient, accumulation of tracer can be seen in cortical target areas such as the frontal cortex, temporal cortex, and precuneus—areas expected to be high in Aβ deposition. In contrast, the HC shows tracer accumulation predominantly in white matter areas. Similar results were obtained for most of the other AD patients and HCs.
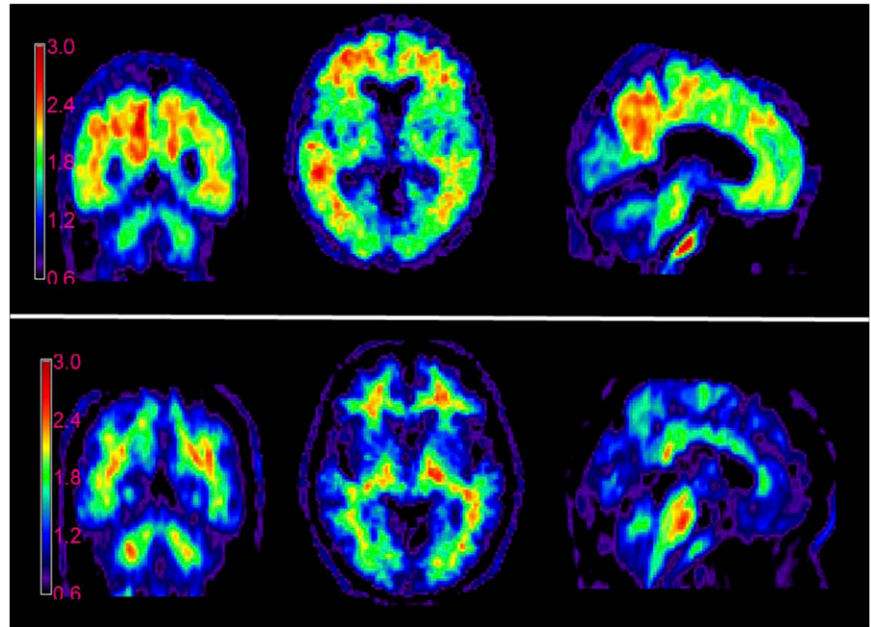
Figure 2 illustrates the average ^{18}F-AV-45 time–activity relationship (SUV units) from 0 to 90 min after the dose administration for AD patients and HCs. ^{18}F-AV-45 was rapidly distributed to the brain of both AD patients and HCs. The tracer was cleared rapidly from the cerebellum (nontarget or reference) VOI of both AD patients and HCs but was selectively retained in cortical target regions, particularly the precuneus, of the AD patients.

Figure 3 shows the average cortical-to-cerebellum SUVR for AD patients and HCs for the 0- to 90-min period. Cortical average SUVRs relative to the cerebellum were higher in AD patients than in HCs. The average cortical-to-cerebellar SUVRs in AD patients show continual substantial increases from 0 to 30 min after administration, with only small changes thereafter, essentially reaching an asymptote by 40–50 min after injection. SUVRs in both AD patients and HCs were relatively constant between 45 and 90 min. Thus, the 10-min period from 50 to 60 min was taken as a representative sample for the asymptotic period.

Table 2 shows the mean SUVRs by cortical region for the 50- to 60-min time frame. The difference in tracer retention between patients with AD and HCs was greatest in the precuneus; SUVRs relative to the cerebellum were 1.86 ± 0.24 and 1.31 ± 0.27 for AD patients and HCs, respectively. In contrast, only a small, relatively inconsistent elevation in tracer retention was observed in the occipital cortex of AD patients. The overall cortical average SUVRs relative to the cerebellum were 1.67 ± 0.18 and 1.25 ± 0.18 for AD patients and HCs, respectively. For both AD patients and HCs, SUVRs relative to the centrum semiovale were lower than SUVRs relative to the cerebellum, but the pattern of separation between AD patients and HCs was similar to that seen with the cerebellar reference region.

Figure 4 shows the precuneus and cortical average SUVRs for the 50- to 60-min time frame for individual AD patients and HCs. Most of the HC values were below the range seen in the AD patients, regardless of subject age. However, in 2 HCs older than 80 y, levels of tracer uptake were similar to those in AD patients; 2 other HCs older than 80 y showed borderline high tracer uptake, particularly in the precuneus. Although none of the AD patients had cortical average SUVRs in the HC range, 1 subject did have relatively low levels of ^{18}F-AV-45 binding in the frontal cortex (not shown) and precuneus.

FIGURE 1. Average of 2 consecutive 5-min ^{18}F-AV-45 PET brain images (obtained 50–60 min after injection of 370 MBq [10 mCi] of ^{18}F-AV-45): 77-y-old woman with mild AD with MMSE of 24 (top) and 82-y-old cognitively healthy man with MMSE of 30 (bottom). Experimental conditions and imaging and computational parameters were identical for the 2 subjects. Counts are shown as ratio to average of gray matter in cerebellum for each subject (SUVR).

Interestingly, this patient had an atypical presentation, including prominent behavior symptoms, gait disturbance, and mild cogwheeling, and was being treated for parkinsonism.

Comparison of SUVR Versus DVR

DVRs were measured in multiple brain regions for a subset of the subjects. Across all centers, the DVR values for individual patients were highly correlated with the corresponding regional SUVR for all regions tested (Spearman ρ ranged from 0.58 for the occipital cortex to 0.88 for the temporal cortex, $P < 0.01$ in all cases).

Radiolabeled Metabolite Analysis of ^{18}F-AV-45

After an injection of ^{18}F-AV-45, the total radioactivity in plasma and the fraction of plasma radioactivity accounted for by ^{18}F-AV-45 were rapidly reduced. Plasma radioactivity was decreased by approximately 80% within 10 min and by approximately 90% within 20 min of injection. In
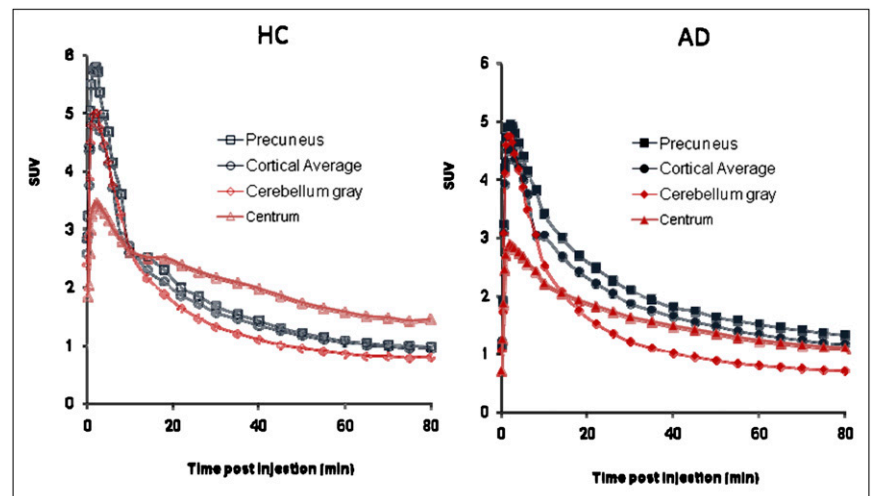
addition to the parent, ^{18}F-AV-45, 3 metabolite peaks were observed. These peaks were matched to cold reference standards and identified as desmethyl-^{18}F-AV-45 (desmethyl ^{18}F-AV-45 can be referred to as ^{18}F-AV-160), N-acetyl-^{18}F-AV-160, and an ^{18}F polar species, the identity of which has not been confirmed.

The supplemental data provide further results pertaining to DVR and SUVR relationships, metabolite analysis, radiation dosimetry and safety.

Whole-Body Radiation Dosimetry

Although the number of subjects and whole-body imaging time points was too few to provide definitive quantitative estimates of radiation dosimetry, preliminary results revealed no unexpected accumulation of tracer. The preliminary estimate of whole-body effective dose was approximately 0.013 mSv/MBq. The organs of excretion—

FIGURE 2. Mean time–activity curves. Mean precuneus, cortical average, and cerebellum SUVs are shown for subjects who were cognitively healthy (HC) and patients with AD. Subjects were scanned for approximately 90 min (horizontal axis represents beginning of each imaging time point, for example, 80–90 min).
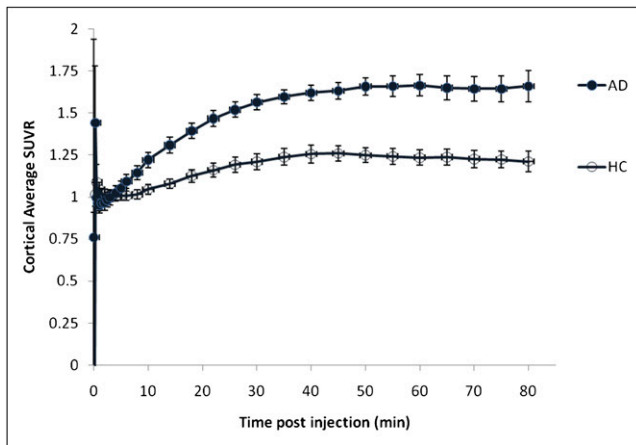
FIGURE 3. Mean cortical average SUVR for subjects who were cognitively healthy (HC) and patients with AD. As would be expected from SUV time–activity curves (Fig. 2), cortical target-to-cerebellum SUVRs for both AD patients and HCs approached asymptote at 50 min and remained essentially unchanged between 50 and 90 min after injection of ^{18}F-AV-45. Subjects were scanned for approximately 90 min (horizontal axis represents beginning of each imaging time point, for example, 80–90 min).

particularly gallbladder, liver, intestines, and urinary bladder—received the greatest exposure.

DISCUSSION

Sixteen AD patients and 16 elderly HCs received ^{18}F-AV-45, with usable imaging data for a total of 11 AD patients and 15 HCs. AD patients showed accumulation of ^{18}F-AV-45 in gray matter cortical target areas expected to be high in Aβ deposition, such as the frontal cortex, temporal cortex, and precuneus. Less consistent tracer accumulation was seen in the occipital cortex, in which Aβ deposition is thought to occur variably and later in the course of the disease. In contrast, HCs showed minimal tracer accumulation, predominantly in white matter areas. This pattern is similar to that previously reported for ^{11}C-PIB (21,22) and ^{18}F-BAY94-9172 (9).

The highest SUVRs were observed in the precuneus of AD patients, and the greatest difference between ^{18}F-AV-45 activity in AD patients and HCs was observed in the precuneus and temporal cortex. This finding is consistent with the known localization of Aβ in these areas in postmortem tissue (23), with recent literature suggesting the precuneus is involved in integrative functions including visual spatial coordination and working memory retrieval (24)—and with results from other Aβ radiotracers (9,25).

The brain kinetics for ^{18}F-AV-45 also appear to be similar to those for ^{11}C-PIB but faster than those for other ^{18}F-labeled Aβ imaging agents such as ^{18}F-BAY94-9172 and ^{18}F-GE-067. The SUV time–activity curves for AD patients (but not HCs) showed a clear separation between cortical and cerebellar activity beginning around 30 min after injection. The average cortical-to-cerebellar SUVRs and the average cortical-to-centrum semiovale SUVRs in AD patients showed continual substantial increases from 0 to 30 min after administration. These SUVRs exhibited only small changes thereafter, reaching a plateau by 40–50 min after injection and remaining stable until at least 90 min after injection. In contrast, other ^{18}F-labeled Aβ imaging agents appear not to reach asymptote until 90 min or more after administration (9,10). The present data suggest that short imaging times (5–10 min) for imaging conducted less than an hour after the administration of ^{18}F-AV-45 will be feasible for routine clinical use.
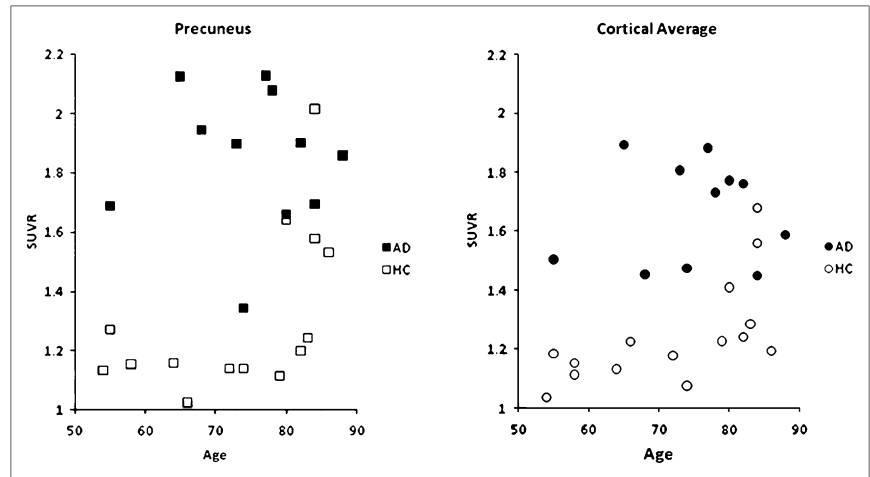
Although there were clear differences in mean cortical-to-cerebellar SUVR between AD patients and HCs, 2 of 15 HCs (13%) showed a pattern of tracer uptake similar to that in AD patients and 2 other HCs showed borderline-high tracer uptake, particularly in the precuneus. Mintun et al. (22) similarly observed AD-like uptake in 10% of controls and borderline-high uptake in another 10% of controls imaged with ^{11}C-PIB. The present findings are also consistent with literature suggesting that 13%−45% of cognitively healthy subjects have significant Aβ pathology at autopsy (26–29). Mintun et al. (22) argued that elevated retention of PET Aβ imaging agents in otherwise cognitively healthy elderly subjects might reflect preclinical AD pathologic changes. However, longitudinal studies will

TABLE 2. SUVRs of Cortical Brain Region Relative to Cerebellum and Centrum Semiovale for 50- to 60-Minute Block: Evaluable Population

Region	Relative to cerebellum		Relative to centrum semiovale	
	AD patients ($n = 11$)	HCs ($n = 15$)	AD patients ($n = 11$)	HCs ($n = 15$)
Frontal cortex	1.67 ± 0.21	1.20 ± 0.30	1.13 ± 0.29	0.68 ± 0.24
Temporal cortex	1.77 ± 0.20	1.31 ± 0.20	1.18 ± 0.24	0.74 ± 0.20
Parietal cortex	1.57 ± 0.27	1.17 ± 0.19	1.05 ± 0.26	0.67 ± 0.17
Anterior cingulate	1.79 ± 0.3	1.30 ± 0.31	1.19 ± 0.28	0.74 ± 0.26
Posterior cingulate	1.65 ± 0.19	1.31 ± 0.21	1.11 ± 0.27	0.74 ± 0.13
Precuneus	1.85 ± 0.24	1.30 ± 0.27	1.25 ± 0.37	0.74 ± 0.23
Occipital cortex	1.36 ± 0.26	1.13 ± 0.13	0.92 ± 0.27	0.64 ± 0.13
Cortical average	1.67 ± 0.18	1.25 ± 0.18	1.12 ± 0.26	0.71 ± 0.18

Data are mean ± SD.

FIGURE 4. Precuneus and cortical average SUVR relative to cerebellum for individual AD patients and cognitively healthy subjects (HC) for all 3 imaging sites.

ultimately be required to determine the significance of such findings for both ^{11}C-PIB and ^{18}F-AV-45.

Although none of the AD patients had cortical average SUVRs in the HC range, 1 presumed AD patient had an HC-like pattern of tracer uptake, particularly in the frontal cortex and precuneus. Interestingly, this AD patient had an unusual presentation, including prominent behavior symptoms, gait disturbance, and mild cogwheeling, and was being treated for parkinsonism. These symptoms, together with the limited tracer uptake, may point to an alternative or additional etiology for the patient's cognitive decline. On the other hand, although this presumed AD patient has an arguably atypical presentation, it would not be unexpected to find low ^{18}F-AV-45 binding or low Aβ burden in some clinically diagnosed AD patients, even with more typical presentations. Literature reports suggest that approximately 10%−20% of patients diagnosed as having probable AD may fail to meet pathologic criteria for AD at autopsy (30–33).

To test the validity of the SUVR analysis used for the present study, DVRs were measured in all brain regions for a subset of the subjects using an analogous but independent set of VOIs and a more sophisticated mathematic modeling approach previously described by Zhou et al. (15). This approach has been successfully used with ^{11}C-PIB and has been useful in demonstrating subtle differences associated with mild cognitive impairment (16). Despite the fact that slightly different VOIs were considered in the 2 approaches (the DVR analysis in this study used the VOIs from the Zhou et al. studies (15,16), rather than the VOIs from the SUVR analysis of this study), the results from the DVR analysis were consistent and highly correlated with the results of the SUVR analysis (Table 3; Supplemental Figs. 2 and 3). DVRs in AD patients were significantly elevated in comparison to DVRs in HCs. Thus, both standard SUVRs during the representative imaging period (50–60 min after the dose administration) and dynamic parametric mapping methods showed significant elevations in ^{18}F-AV-45 in several brain regions of AD patients, compared with HCs. These findings provide strong

cross validation for the methods and results (and the VOIs) obtained via the SUVR analysis. In our companion paper, we (Paul B. Rosenberg, Dean F. Wong, Steven Edell, et al., submitted 2010) will report on the relationship between behavioral and neuropsychologic measures and ^{18}F-AV-45 for both SUVs and some DVR measures.

Tracer plasma kinetics and metabolism were also examined in this study (supplemental materials). Although brain SUVs reached a plateau at 50–60 min of around 20% (in nontarget tissue) to 40% of initial levels (in Aβ-containing cortical tissue of AD patients), plasma radioactivity was reduced to less than 10% of the initial level by 20 min after injection (Supplemental Fig. 4). Because of the rapid clearance of total radioactivity from plasma, it seems unlikely that plasma levels of radioactive metabolite could be high enough to account for the observed tracer activity in the brain. The supplemental material provides additional information.

TABLE 3. Average and SD of DVRs in AD Patients and HCs

Region	AD patients		HCs	
	Average	SD	Average	SD
Frontal*	1.41	0.17	1.14	0.21
Temporal*	1.37	0.13	1.14	0.12
Parietal†	1.42	0.20	1.20	0.13
Occipital†	1.31	0.20	1.09	0.12
Fusiform gyrus*	1.17	0.11	1.01	0.07
Cingulate*	1.55	0.15	1.25	0.23
Pons	1.47	0.11	1.51	0.09
Parahippocampus†	1.16	0.11	1.04	0.07
Hippocampus	1.09	0.17	1.06	0.07
Insula*	1.41	0.15	1.16	0.17
Putamen†	1.60	0.18	1.39	0.16
Caudate nucleus†	1.38	0.21	1.15	0.21
Thalamus	1.35	0.19	1.35	0.12

*By simple *t* test (no corrections for multiple comparisons) AD DVR was significantly greater than HC DVR, $P < 0.05$.
†AD DVR greater than HC DVR, $0.1 < P > 0.05$.
Data are for JHU group only.

^{18}F-AV-45 was shown to be well tolerated in the population studied (supplemental material). No serious adverse events or clinically significant changes in laboratory or electrocardiogram parameters were observed. Additionally, whole-body imaging revealed no unexpected accumulation of tracer.

A weakness of the present study is that the number of subjects and whole-body imaging time points was too few to provide definitive quantitative estimates of radiation dosimetry. However, a subsequent study evaluated whole-body exposure for up to 6 h after the administration of ^{18}F-AV-45. A preliminary report (34) confirmed the present finding that the organs of excretion—particularly the gallbladder, liver, intestines, and urinary bladder—received the greatest radiation exposure.

A second potential weakness of the study is that 6 of 32 planned subjects were not included in the primary analysis. Data from the first HC were lost because of PET scanner problems; 1 AD withdrew consent, and 4 of 16 AD patients exhibited significant movement during the 90-min scanning. Because this was a first study in humans, designed to evaluate the potential of ^{18}F-AV-45 for future development, the decision was made to focus only on the 26 images that could be accurately quantified with minimal movement artifacts and attenuation error. On visual examination, the images of the 4 excluded AD patients were not atypical, but accurate quantification of these images was precluded by potential attenuation error.

These imaging failures illustrate the need for a simple and brief acquisition procedure when imaging AD patients in a community setting. In the present study, scans averaged over a 10-min period beginning 50 min after injection were sufficient to reliably distinguish ^{18}F-AV-45 binding in AD patients from that in HCs in each of the relevant cortical areas (Table 2). Additionally, Figure 3 suggests that scans as short as 5 min could be effective. Moreover, because AD and HC SUVRs appear stable between 40 and 90 min, an opportunity may exist to reposition and repeat a scan if a patient moves or a technical error occurs during the initial 10-min scan.

CONCLUSION

^{18}F-AV-45 was shown in this first study in humans to be well tolerated, with no serious adverse events. The cortical target regions in patients with AD had higher uptake of ^{18}F-AV-45 over time than did regions in subjects who were cognitively healthy. The greatest increase in uptake occurred in the precuneus and temporal cortex of AD patients, compared with HCs. Scans 50–60 min after injection produced reliable imaging results. ^{18}F-AV-45—given its relatively long radioactive half-life, relatively rapid kinetics (requiring a short postdose waiting period and short imaging durations), and relatively long, stable plateau (providing flexibility in timing of the image)—may be a robust imaging tool and potentially well suited as a biomarker for AD in large multicenter treatment and natural history trials (e.g.,

Alzheimer's Disease Neuroimaging Initiative) and for imaging in community settings.

REFERENCES

1. Selkoe DJ. Defining molecular targets to prevent Alzheimer disease. *Arch Neurol.* 2005;62:192–195.
2. Hyman BT, Trojanowski JQ. Consensus recommendations for the postmortem diagnosis of Alzheimer disease from the National Institute on Aging and the Reagan Institute Working Group on diagnostic criteria for the neuropathological assessment of Alzheimer disease. *J Neuropathol Exp Neurol.* 1997;56:1095–1097.
3. Mirra SS, Heyman A, McKeel D, et al. The Consortium to Establish a Registry for Alzheimer's Disease (CERAD): Part II. Standardization of the neuropathologic assessment of Alzheimer's disease. *Neurology.* 1991;41:479–486.
4. Hock C, Konietzko U, Streffer JR, et al. Antibodies against β-amyloid slow cognitive decline in Alzheimer's disease. *Neuron.* 2003;38:547–554.
5. Pike KE, Savage G, Villemagne VL, et al. β-amyloid imaging and memory in non-demented individuals: evidence for preclinical Alzheimer's disease. *Brain.* 2007;130:2837–2844.
6. Fagan AM, Roe CM, Xiong C, Mintun MA, Morris JC, Holtzman DM. Cerebrospinal fluid tau/β-amyloid$_{42}$ ratio as a prediction of cognitive decline in nondemented older adults. *Arch Neurol.* 2007;64:343–349.
7. Klunk WE, Wang Y, Huang GF, Debnath ML, Holt DP, Mathis CA. Uncharged thioflavin-T derivatives bind to amyloid-β protein with high affinity and readily enter the brain. *Life Sci.* 2001;69:1471–1484.
8. Small GW, Kepe V, Ercoli LM, et al. PET of brain amyloid and tau in mild cognitive impairment. *N Engl J Med.* 2006;355:2652–2663.
9. Rowe CC, Ackerman U, Browne W, et al. Imaging of amyloid βin Alzheimer's disease with ^{18}F-BAY94-9172, a novel PET tracer: proof of mechanism. *Lancet Neurol.* 2008;7:129–135.
10. Koole M, Lewis DM, Buckley C, et al. Whole-body biodistribution and radiation dosimetry of ^{18}F-GE067: a radioligand for in vivo brain amyloid imaging. *J Nucl Med.* 2009;50:818–822.
11. Choi SR, Golding G, Zhuang ZP, et al. Preclinical properties of ^{18}F-AV-45: a PET agent for Aβ plaques in the brain. *J Nucl Med.* 2009;50:1887–1894.
12. Alzheimer's Association. Research consent for cognitively impaired adults: recommendations for institutional review boards and investigators. *Alzheimer Dis Assoc Disord.* 2004;18:171–175.
13. Folstein MF, Folstein SE, McHugh PR. "Mini-mental state": a practical method for grading the cognitive state of patients for the clinician. *J Psychiatr Res.* 1975;12:189–198.

14. Hilton J, Yokoi F, Dannals RF, Ravert HT, Szabo Z, Wong DF. Column-switching HPLC for the analysis of plasma in PET imaging studies. *Nucl Med Biol.* 2000;27:627–630.

15. Zhou Y, Endres CJ, Brasic JR, Huang SC, Wong DF. Linear regression with spatial constraint to generate parametric images of ligand-receptor dynamic PET studies with a simplified reference tissue model. *Neuroimage.* 2003;18:975–989.

16. Zhou Y, Resnick SM, Ye W, et al. Using a reference tissue model with spatial constraint to quantify [11C]Pittsburgh compound B PET for early diagnosis of Alzheimer's disease. *Neuroimage.* 2007;36:298–312.

17. Foster D, Barrett P. Developing and testing integrated multicompartment models to describe a single-input multiple-output study using the SAAM II software system. In: *Proceedings of the Sixth International Radiopharmaceutical Dosimetry Symposium.* Oak Ridge, TN: Oak Ridge Institute for Science and Education; 1998.

18. Stabin MG, Siegel JA. Physical models and dose factors for use in internal dose assessment. *Health Phys.* 2003;85:294–310.

19. Stabin MG, Sparks RB, Crowe E. OLINDA/EXM: the second-generation personal computer software for internal dose assessment in nuclear medicine. *J Nucl Med.* 2005;46:1023–1027.

20. International Commission on Radiological Protection (ICRP). *Limits for Intakes of Radionuclides by Workers.* Oxford, U.K.: Pergamon Press; 1979.

21. Lopresti BJ, Klunk WE, Mathis CA, et al. Simplified quantification of Pittsburgh Compound B amyloid imaging PET studies: a comparative analysis. *J Nucl Med.* 2005;46:1959–1972.

22. Mintun MA, Larossa GN, Sheline YI, et al. [11C]PIB in a nondemented population: potential antecedent marker of Alzheimer disease. *Neurology.* 2006; 67:446–452.

23. Braak H, Braak E. Staging of Alzheimer-related cortical destruction. *Int Psychogeriatr.* 1997;9(suppl 1):257–261.

24. Cavanna AE, Trimble MR. The precuneus: a review of its functional anatomy and behavioral correlates. *Brain.* 2006;129:564–583.

25. Ziolko SK, Weissfeld LA, Klunk WE, et al. Evaluation of voxel-based methods for the statistical analysis of PIB PET amyloid imaging studies in Alzheimer's disease. *Neuroimage.* 2006;33:94–102.

26. Schmitt FA, Davis DG, Wekstein DR, Smith CD, Ashford JW, Markesbery WR. "Preclinical" AD revisited: neuropathology of cognitively normal older adults. *Neurology.* 2000;55:370–376.

27. Price JL, Morris JC. Tangles and plaques in nondemented aging and "preclinical" Alzheimer's disease. *Ann Neurol.* 1999;45:358–368.

28. Knopman DS, Parisi JE, Salviati A, et al. Neuropathology of cognitively normal elderly. *J Neuropathol Exp Neurol.* 2003;62:1087–1095.

29. Hulette CM, Welsh-Bohmer KA, Murray MG, Saunders AM, Mash DC, McIntyre LM. Neuropathological and neuropsychological changes in "normal" aging: evidence for preclinical Alzheimer disease in cognitively normal individuals. *J Neuropathol Exp Neurol.* 1998;57:1168–1174.

30. Gearing M, Mirra SS, Hedreen JC, Sumi SM, Hansen LA, Heyman A. The Consortium to Establish a Registry for Alzheimer's Disease (CERAD): Part X. Neuropathology confirmation of the clinical diagnosis of Alzheimer's disease. *Neurology.* 1995;45:461–466.

31. Lim A, Tsuang D, Kukull W, et al. Clinico-neuropathological correlation of Alzheimer's disease in a community-based case series. *J Am Geriatr Soc.* 1999; 47:564–569.

32. Mok W, Chow TW, Zheng L, Mack WJ, Miller C. Clinicopathological concordance of dementia diagnoses by community versus tertiary care clinicians. *Am J Alzheimers Dis Other Demen.* 2004;19:161–165.

33. Pearl GS. Diagnosis of Alzheimer's disease in a community hospital-based brain bank program. *South Med J.* 1997;90:720–722.

34. Adler LP, Wolodzko J, Stabin M, McNelis T, Gammage LL, Joshi A. Radiation dosimetry of 18FAV-45 measured by PET/CT in humans [abstract]. *J Nucl Med.* 2008;49(suppl 1):283P.